Development 137, 4307-4316 (2010) doi:10.1242/dev.052647

The neural crest-enriched microRNA miR-452 regulates epithelial-mesenchymal signaling in the first pharyngeal arch

Neil T. Sheehy[1,2,3,*], Kimberly R. Cordes[1,2,3,*], Mark P. White[1,2,3], Kathryn N. Ivey[1,2] and Deepak Srivastava[1,2,3,†]

SUMMARY

Neural crest cells (NCCs) are a subset of multipotent, migratory stem cells that populate a large number of tissues during development and are important for craniofacial and cardiac morphogenesis. Although microRNAs (miRNAs) have emerged as important regulators of development and disease, little is known about their role in NCC development. Here, we show that loss of miRNA biogenesis by NCC-specific disruption of murine *Dicer* results in embryos lacking craniofacial cartilaginous structures, cardiac outflow tract septation and thymic and dorsal root ganglia development. *Dicer* mutant embryos had reduced expression of *Dlx2*, a transcriptional regulator of pharyngeal arch development, in the first pharyngeal arch (PA1). miR-452 was enriched in NCCs, was sufficient to rescue *Dlx2* expression in *Dicer* mutant pharyngeal arches, and regulated non-cell-autonomous signaling involving *Wnt5a*, *Shh* and *Fgf8* that converged on *Dlx2* regulation in PA1. Correspondingly, knockdown of miR-452 in vivo decreased *Dlx2* expression in the mandibular component of PA1, leading to craniofacial defects. These results suggest that post-transcriptional regulation by miRNAs is required for differentiation of NCC-derived tissues and that miR-452 is involved in epithelial-mesenchymal signaling in the pharyngeal arch.

KEY WORDS: microRNA, Neural crest, Pharyngeal arch, Epithelial-mesenchymal interaction, Dicer (Dicer1), Mouse

INTRODUCTION

The proper migration and differentiation of neural crest cells (NCCs) is essential for craniofacial, cardiac, peripheral and enteric nervous system, melanocyte and thymic development (Helms and Schneider, 2003; Jiang et al., 2000; Le Douarin et al., 2004; Lee et al., 2004a). After delaminating from the dorsal portion of the neural tube, NCCs migrate ventrolaterally along stereotypical routes and are induced to differentiate through reciprocal signaling with neighboring cells (Sauka-Spengler and Bronner-Fraser, 2008). Cranial NCCs populate the pharyngeal arches (PAs), where the neural crest-derived mesenchyme encounters a number of instructive signals from the pharyngeal epithelia (i.e. endoderm and ectoderm), resulting in differentiation into the proper cell lineages (Kameda, 2009; Le Douarin et al., 2004). Similarly, NCCs that populate the outflow tract of the heart and the developing aortic arch arteries rely on reciprocal signaling with neighboring cardiac progenitor cells derived from the second heart field (Waldo et al., 2005). Disruption of NCC development, cell- or non-cell-autonomously, results in numerous forms of human birth defects, including DiGeorge and Treacher-Collins syndromes (Epstein and Parmacek, 2005). Although many signaling pathways and transcription factors involved in NCC development are known (Meulemans and Bronner-Fraser, 2004; Trainor et al., 2002), the mechanism by which post-transcriptional regulation affects NCC development has not been established.

MicroRNAs (miRNAs) are an important class of post-transcriptional regulatory molecules. They typically bind to sequence-specific binding sites within the 3′-untranslated region (3′-UTR) of target mRNAs to repress translation, degrade the target message, or both (Bartel, 2009). The RNase III enzyme Dicer is required for the cleavage of precursor miRNAs into fully functional, mature miRNAs (Lee et al., 2004b). Studies with specific miRNA and conditional *Dicer* deletions have revealed that miRNAs are required for the proper development of a number of tissues, including lungs, cardiac muscle, cartilage, skin and limbs (Harris et al., 2006; van Rooij et al., 2007; Zhao et al., 2007; Kobayashi et al., 2008; Yi et al., 2009; Harfe et al., 2005). Deletion of *Dicer* in NCCs disrupts proper cranial NCC development (Zehir et al., 2010); however, the individual miRNAs that contribute to neural crest development and the mechanism by which they do so remain unknown.

Here, we show that disruption of miRNA biogenesis in NCCs not only affects cranial and cardiac neural crest development, but also specifically affects the expression of *Dlx2* in the mandibular component of the first pharyngeal arch (PA1). We profiled miRNAs enriched in NCCs and found that one NCC-enriched miRNA, miR-452, was sufficient to rescue proper expression of *Dlx2*, a known PA patterning gene, in the mandibular component of PA1. Additionally, we found that miR-452 regulated reciprocal epithelial-mesenchymal signaling in PA1 involving Wnt5a, Shh and Fgf8 converging on *Dlx2* expression. Thus, our study reveals a novel miRNA-regulated signaling cascade within NCCs and the pharyngeal apparatus.

MATERIALS AND METHODS

Mating and genotyping mice

Dicer$^{flox/flox}$ mice (Harfe et al., 2005) and *Wnt1-cre* mice (Danielian et al., 1998) were intercrossed to generate *Dicer*$^{flox/flox}$ *Wnt1-cre* mice. Genotyping was performed by PCR with primers: Cre1, 5′-AGGTCCGTTCACTCATGGA-3′; Cre2, 5′-TCGACCAGTTTA-GTTACCC-3′; Dicer-For, 5′-ATTGTTACCAGCGCTTAGAATTCC-3′;

[1]Gladstone Institute of Cardiovascular Disease, San Francisco, CA 94158, USA.
[2]Department of Pediatrics, University of California, San Francisco, CA 94143, USA.
[3]Department of Biochemistry and Biophysics, University of California, San Francisco, CA 94143, USA.

*These authors contributed equally to this work
†Author for correspondence (dsrivastava@gladstone.ucsf.edu)

Accepted 14 October 2010

and Dicer-Rev, 5′-GTACGTCTACAATTGTCTATG-3′. *ROSA26* reporter *(R26R)-YFP* mice (Jackson Laboratory, Bar Harbor, ME, USA) were bred with $Dicer^{flox/flox}$ mice to generate $Dicer^{floxP/+}$ *R26R-YFP* mice.

Histological analysis

Skeletons from embryos were stained with Alcian Blue as described (McLeod, 1980). Yellow latex cast dye (Connecticut Valley Biological Supply, South Hampton, MA, USA) was injected into the beating left ventricle of wild-type or mutant hearts with a 30 1/2 gauge needle. The hearts were dehydrated and cleared in benzyl benzoate:benzyl alcohol (2:1) to visualize the yellow latex in the vasculature. Pregnant mothers were dissected to obtain E13-14.5 wild-type and mutant embryos, which were fixed in 10% formalin and paraffin embedded. Transverse sections through the heart and brain were stained with Hematoxylin and Eosin (H&E) to analyze morphology, 1:500 rabbit anti-NF-M antibody (Abcam, Cambridge, MA, USA) to visualize neuronal tissue, 1:100 rabbit anti-GFP antibody (Sigma-Aldrich, St Louis, MO, USA) to visualize NCC progeny, and 1:500 Cy5-conjugated mouse anti-smooth muscle actin (SMA) (Sigma) to visualize smooth muscle cells. Apoptosis assays were performed using the TUNEL Assay Kit (Roche, Indianapolis, IN, USA). Proliferation studies were performed using the Phospho-Histone $H3^{(ser10)}$ Assay (Millipore, Billerica, MA, USA).

In situ hybridization

mRNA in situ hybridization of whole-mount embryos was carried out as described (Riddle et al., 1993) with digoxigenin-labeled probes, which were synthesized with Digoxigenin Labeling Mix (Roche) and T7 or T3 RNA polymerase (Roche). The Msx1, Dlx2, Gli1 and Fgf8 riboprobes have been described (Thomas et al., 1998; Lee et al., 1997; Meyers and Martin, 1999). Briefly, embryos were collected at E10.5, fixed in 4% paraformaldehyde and dehydrated in 100% methanol. Before hybridization, embryos were rehydrated, treated with 10 μg/ml proteinase K (Sigma-Aldrich) for 15 minutes, and placed in prehybridization buffer for 2 hours at 70°C. Probes (0.5 μg/ml) were added and embryos were hybridized overnight at 70°C. After a series of washing steps, digoxigenin was detected with an anti-digoxigenin antibody conjugated with alkaline phosphatase (Roche). Color development was visualized with BM Purple substrate (Roche), and images were obtained with a Leica microscope.

Flow sorting and miRNA microarray

Embryos from $Wnt1^{Cre}$ or $Dicer^{flox/+}$ $Wnt1^{Cre}$ mice intercrossed with *R26R-YFP* mice were collected at E10.5 and E11.5, dissected and trypsinized. The cells were spun at 2000 rpm (425 ***g***) and the pellet was resuspended in PBS and filtered through a 40-μm membrane (Millipore). Selection by FACS was based on YFP expression. YFP^+ (10,000-30,000 cells per embryo) and YFP^- (50,000-100,000 cells per embryo) cells were collected, total RNA was isolated using Trizol (Invitrogen, Carlsbad, CA, USA), and 1 μg of RNA for each cell population was used for miRNA microarray hybridizations (Exiqon, Denmark). Array data were analyzed using R/Bioconductor Bioinformatic software (Gentleman et al., 2004) and the marray package. GenePix (Axon) flagged spots were removed and only unflagged mmu-miR probes were used for normalization and subsequent analysis. Cy5/Cy3 signals were calculated for each array and normalized by loess normalization (Yang et al., 2002). Microarray data are available at Gene Expression Omnibus under accession number GSE25256.

Pharyngeal arch culture

PAs were cultured according to the modified Sanger method (Trowell, 1954). Briefly, PAs from mutant and control embryos were dissected at E9.5 and incubated with 2 U/ml dispase to dissociate the epithelial layer from the mesenchymal cells. The epithelial layer was further permeabilized with fine tungsten needles, and the PAs were placed on a nitrocellulose membrane (Millipore) supported by a wire frame. The apparatus was placed in BGJb medium (Gibco, Carlsbad, CA, USA) supplemented with 50 U/ml penicillin/streptomycin and kept at 37°C for 48 hours.

Dlx2 rescue experiments were carried out in cultured PAs co-transfected with 66 pmol 2′O-methyl oligoribonucleotide mimics (miR-452 or miR-513; Dharmacon, LaFayette, CO, USA) and 33 pmol Block-iT Alexa Fluor-red fluorescent control oligo (Invitrogen) with Lipofectamine 2000 (Invitrogen). After 48 hours, PAs were fixed in 4% paraformaldehyde and dehydrated in 100% methanol for in situ hybridization or in Trizol for quantitative (q) RT-PCR.

Affi-Gel beads (Bio-Rad) were incubated in 200 ng/μl recombinant Wnt5a protein (R&D Systems, Minneapolis, MN, USA) or bovine serum albumin (BSA) (Invitrogen) for 2 hours at 37°C. During incubation, the PA1s from E10.5 *Ptch1-lacZ* (Jackson Laboratory) mouse embryos were dissected and prepared for explant culture as described, excluding the dispase treatment. Beads were then transplanted into the mesenchyme with fine tungsten needles and cultured for 36 hours. The PAs were then fixed in 4% paraformaldehyde and stained for β-galactosidase (β-Gal) activity. Similar experiments were performed in wild-type embryos assaying *Dlx2* mRNA expression in response to Wnt5a-soaked beads.

qRT-PCR

RNA was prepared from PAs transfected with miR-452 mimic and Block-iT Alexa Fluor-red (Invitrogen) or Block-iT alone, using Trizol. For miRNA qRT-PCR, cDNA was reverse transcribed from 10 ng total RNA using the TaqMan microRNA Reverse Transcription Kit (Applied Biosystems, Foster City, CA, USA). miR-16 and U6 small nuclear RNA served as endogenous controls.

In vivo antagomir injections

Wild-type FVB mice (Jackson Laboratory) were mated and plugs were identified; noon of the day of plug discovery was considered E0.5. At E8.5, pregnant mothers were anesthetized with isofluorane. A small incision was made in the abdomen and the uterus was carefully pulled through the incision to reveal the ovaries. A NanoFil syringe (World Precision Instruments) fitted with a 35-gauge beveled needle was filled with PBS (control) or 3 mg/ml miR-452 antagomir (Dharmacon) diluted in PBS. Using a microsyringe pump (World Precision Instruments), 3 μl was injected into the embryonic space through the intact deciduum of each embryo. After all embryos had been injected, the uterus was carefully placed back into the pregnant mother and the incision was closed with sutures. The embryos were allowed to develop to E11.5 or E16.5 and harvested for in situ hybridization, qRT-PCR or histological analysis.

Joma1.3 cell culture

Joma1.3 cells were cultured as described (Maurer et al., 2007). Briefly, cells were plated on cell culture dishes coated with 1 mg/ml fibronectin (Roche) in a 1:1 mixture of Dulbecco's modified Eagle's medium and F12 medium (Gibco) containing 1% N2 supplement (Invitrogen), 2% B27 supplement (Invitrogen), 10 ng/ml epidermal growth factor (Invitrogen), 1 ng/ml fibroblast growth factor (Invitrogen), 100 U/ml penicillin/streptomycin (Invitrogen) and 10% chick embryo extract (Stemple and Anderson, 1992). To maintain cells in an undifferentiated state, 200 nM 4-OHT (Sigma-Aldrich) was added fresh to the medium.

Luciferase assays to determine putative targets were performed with undifferentiated Joma1.3 cells. A ~500 bp fragment containing the predicted miR-452 binding site for each predicted mRNA target was cloned into pMIR-Report luciferase reporter vectors (Applied Biosystems). For the luciferase assays for the mutant Wnt5a binding site, oligos for 50 bp surrounding the wild-type Wnt5a binding site (mouse chromosome 14: 29338052-74) or mutant binding site (corresponding to bases 3-6 in the seed sequence of miR-452, mutated from CAA to TCG) were annealed together to form concatamers consisting of five consecutive binding sites. These were then cloned into pMIR-Report luciferase reporter vectors. All assays were performed in triplicate in 12-well plates with Joma1.3 cells transfected with Lipofectamine 2000. After 24 hours in culture, cells were harvested and luciferase intensity was measured with the Luciferase Dual-Reporter Assay (Promega) and normalized to *Renilla* luciferase.

For Shh responsiveness assays, hsa-Wnt5a cDNA (Open Biosystems, Hunstville, AL, USA) was cloned into pEF6-V5 expression vectors (Invitrogen). Joma1.3 cells were transfected with Lipofectamine 2000. After 24 hours in culture, 0.5 μg/ml recombinant Shh-N protein (R&D Systems) was added to the medium and the cells were cultured for 24 hours. Cells were then harvested, RNA isolated and qRT-PCR performed to determine relative gene expression levels.

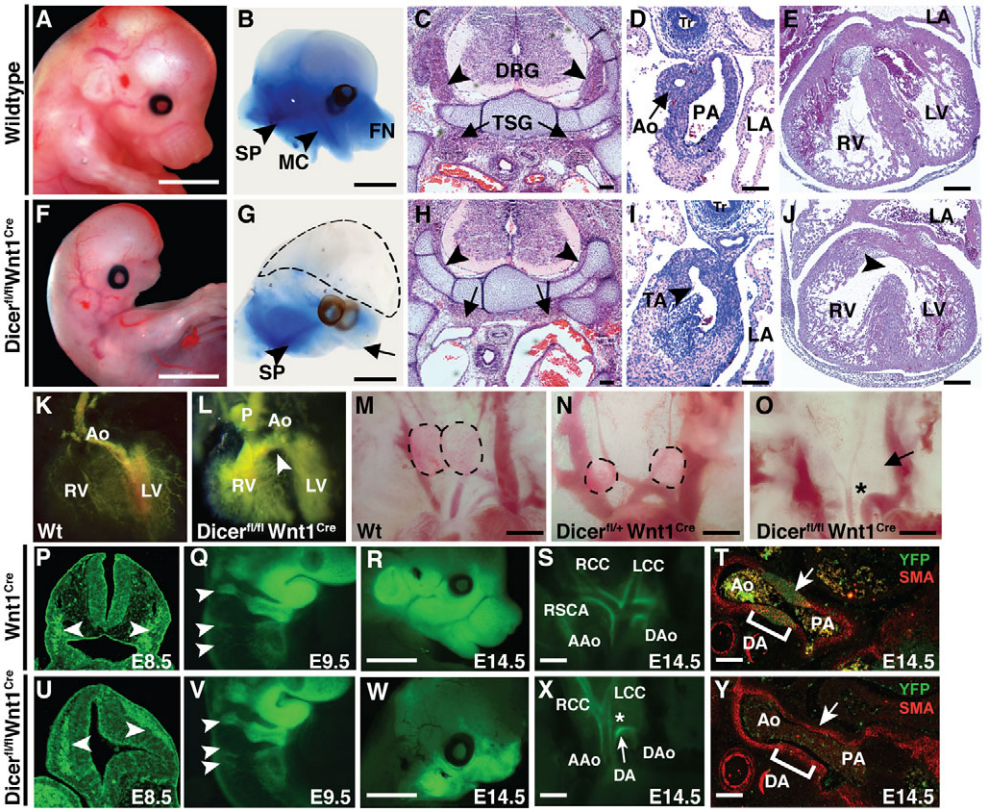

Fig. 1. Phenotypic analysis of *Dicer*$^{flox/flox}$ *Wnt1*^{Cre} mutant mouse embryos. (**A**,**F**) Lateral view of E14.5 wild-type (A) and *Dicer*$^{flox/flox}$ *Wnt1*^{Cre} mutant (F) mouse embryos. (**B**,**G**) Cartilage staining with Alcian Blue shows loss of craniofacial cartilaginous tissue (dashed line, arrow) in *Dicer* mutants (G) but not wild-type embryos (B). Note the presence of the styloid process (SP) and absence of the Meckel's cartilage (MC) and frontonasal cartilage (FN). (**C**,**H**) H&E staining of transverse sections from E13.5 wild-type (C) and *Dicer* mutant (H) embryos showing loss of dorsal root ganglia (DRG, arrowheads) and thoracic sympathetic ganglia (TSG, arrows). (**D**,**I**) Transverse sections of the outflow tract region at E14.5 show normal septation of the pulmonary artery (PA) and aorta (Ao) in wild-type embryos (D), but communication between the two vessels remains, reflecting a truncus arteriosus (TA) in *Dicer* mutants (I). Tr, trachea; LA, left atrium. (**E**,**J**) Transverse sections of the right (RV) and left (LV) ventricles of E14.5 wild type (E) and *Dicer* mutant (J). Arrowhead indicates ventricular septal defect. (**K**,**L**) Latex injections into the left ventricle of E14.5 embryonic hearts show a ventricular septal defect (arrowhead) in *Dicer* mutants (L) versus wild type (Wt; K), with latex flow from the left to right ventricle. (**M-O**) Brightfield images of thymus (dashed lines; image is contrast enhanced to visualize thymus) from E14.5 wild-type (M), *Dicer*$^{flox/+}$ *Wnt1*^{Cre} heterozygous (N), and *Dicer*$^{flox/flox}$ *Wnt1*^{Cre} mutant (O) embryos. Arrow indicates absence of thymus in mutant. Asterisk (O) indicates the interrupted communication between the ascending aorta and descending aorta. (**P**,**U**) Transverse sections of E8.5 *Dicer*$^{+/+}$ *Wnt1*^{Cre} *R26R*^{YFP} (P) and *Dicer*$^{flox/flox}$ *Wnt1*^{Cre} *R26R*^{YFP} (U) embryos through the neural tube showing lineage tracing of NCCs. Arrowheads indicate migrating streams of NCCs. (**Q**,**V**) Lateral view of E9.5 pharyngeal arch (PA) region of *Dicer*$^{+/+}$ *Wnt1*^{Cre} *R26R*^{YFP} (Q) and *Dicer*$^{flox/flox}$ *Wnt1*^{Cre} *R26R*^{YFP} (V) embryos showing lineage tracing of NCCs. Arrowheads indicate migrating streams of NCCs. (**R**,**W**) Lateral view of the craniofacial region of E14.5 *Dicer*$^{+/+}$ *Wnt1*^{Cre} *R26R*^{YFP} (R) and *Dicer*$^{flox/flox}$ *Wnt1*^{Cre} *R26R*^{YFP} (W) embryos. (**S**,**X**) Images of the outflow tracts and aortic arch. Asterisk denotes absence of the transverse aorta in the mutant (X, see also O), with the vascular connection to the descending aorta being the ductus arteriosus (DA). RCC, right common carotid artery; LCC, left common carotid artery; RSCA, right subclavian artery; AAo, ascending aorta; DAo, descending aorta. (**T**,**Y**) Immunofluorescence of transverse sections through the aortic arch of S and X, respectively, stained for GFP (green) and smooth muscle actin (SMA, red). Arrow (Y) indicates the absence of NCC-derived smooth muscle cells in the wall of the ductus arteriosus as is present in T, connecting the aorta and PA. Scale bars: 2 mm in A,B,F,G; 100 μm C-E,H-Y.

Western blots were performed using lysate from Joma1.3 cells or PA explant culture with or without transfection of 66 pmol miR-452 mimic and immunoblotted with goat anti-Wnt5a antibody (R&D Systems) and quantified using the LI-COR Odyssey Imaging System (LI-COR Biosciences, Lincoln, NE, USA).

RESULTS

Dicer$^{flox/flox}$ *Wnt1*^{Cre} mutant mouse embryos have defective craniofacial, cardiovascular and thymic development

To determine whether miRNA biogenesis is required for the proper development of NCCs, we disrupted the miRNA-processing enzyme Dicer (Dicer1 – Mouse Genome informatics) with a *Dicer* allele in which the exon encoding the second RNase III domains was flanked by loxP sites (Harfe et al., 2005). We crossed *Wnt1*^{Cre} transgenic mice, in which Cre recombinase is expressed in pre-migratory NCC progenitors and progeny at embryonic day (E) 8.5 (Danielian et al., 1998), with *Dicer*$^{flox/flox}$ mice. Embryos lacking *Dicer* in NCCs had severe defects in the development of NCC-derived tissues and died soon after E16.5. In mutants, severe craniofacial defects were apparent by E14.5 (Fig. 1A,F). The NCC-derived maxillary and mandibular regions of the face and the frontonasal process lacked cartilaginous tissue (Fig. 1B,G). However, the presence of mesodermally derived cartilage near the base of the skull and non-NCC-derived tissue in the head (Fig. 1G, dashed lines) suggested that the defects were mainly restricted to

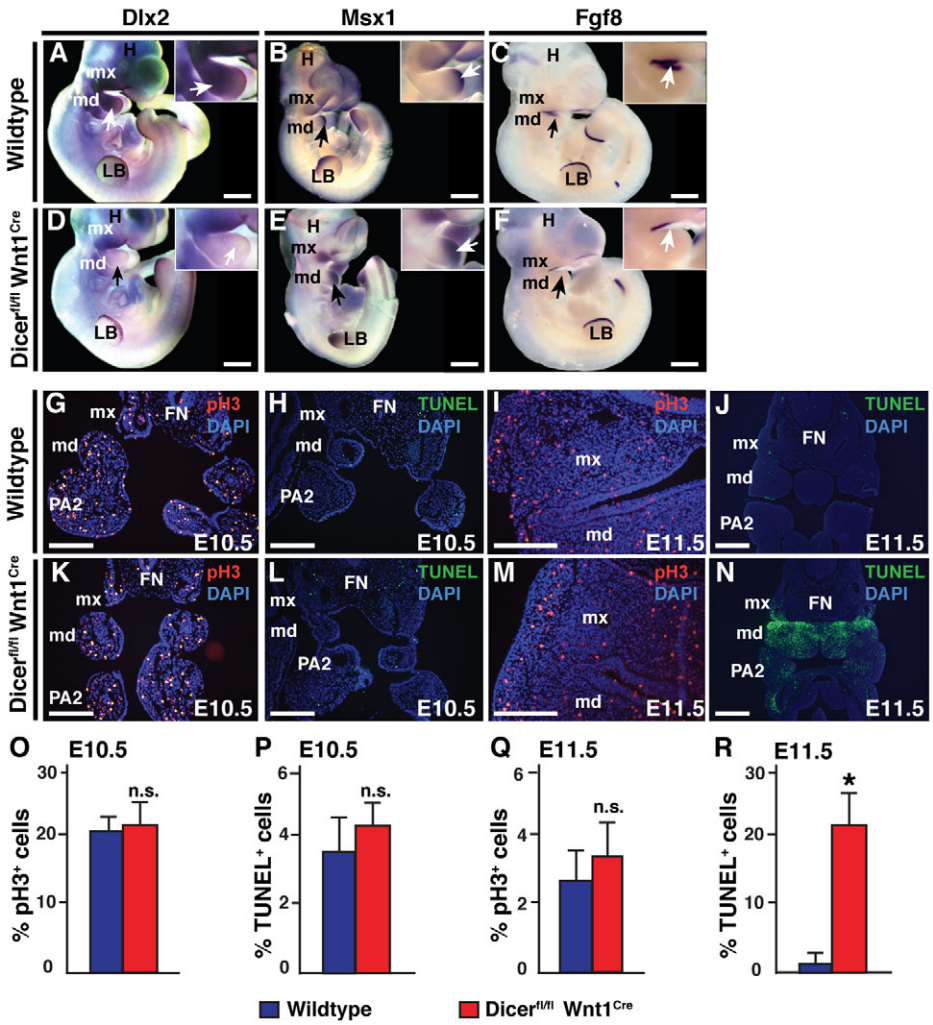

Fig. 2. *Dicer*$^{flox/flox}$ *Wnt1*^{Cre} mutant mouse embryos have decreased *Dlx2* and *Fgf8* expression and increased cell death in PA1. (**A-F**) In situ hybridization of E10.5 wild-type (A-C) and *Dicer* mutant (D-F) embryos for expression of *Dlx2* (A,D), *Msx1* (B,E) and *Fgf8* (C,F). Arrows indicate the mandibular component of PA1 and insets are higher magnification views of this region. (**G**,**K**,**O**) Phospho-histone H3 (pH3) immunohistochemistry to assay proliferating cells of representative frontal sections from E10.5 wild-type (G) and *Dicer* mutant (K) mouse embryos, quantified from multiple sections (O). (**H**,**L**,**P**) TUNEL assay to quantify apoptotic cells of representative frontal sections from E10.5 wild-type (H) and *Dicer* mutant (L) mouse embryos, quantified from multiple sections (P). (**I**,**M**,**Q**) pH3 immunohistochemistry to assay proliferating cells of representative frontal sections from E11.5 wild-type (I) and *Dicer* mutant (M) mouse embryos, quantified from multiple sections (Q). (**J**,**N**,**R**) TUNEL assay in frontal sections of E11.5 wild-type (J) and *Dicer* mutant (N) embryos, quantified from multiple sections (R). Error bars indicate 95% confidence intervals. n.s., not statistically significant; **P*<0.05. mx, maxillary component of PA1; md, mandibular component of PA1; PA2, second PA; H, head; LB, limb bud; FN, frontonasal process. Scale bars: 500 μm for A-F; 200 μm for G-N.

NCC-derived cartilages at E14.5. We also observed loss of NCC-derived neuronal tissue from the dorsal root ganglia (DRG) and thoracic sympathetic ganglia (TSG) in *Dicer*$^{flox/flox}$ *Wnt1*^{Cre} mutants by staining with H&E or the pan-neuronal marker neurofilament-M (NF-M; Nefm – Mouse Genome informatics) (Fig. 1C,H and see Fig. S1A,B in the supplementary material).

In addition to defective craniofacial and neuronal development, we also observed defects in the development of other NCC-derived tissues. In some cases, the outflow tract did not fully septate into a pulmonary artery and aorta, resulting in the persistence of a common outflow vessel (truncus arteriosus) (Fig. 1D,I). In humans, persistent truncus arteriosus is a consequence of NCC defects and is often accompanied by a ventricular septal defect and patterning defects of the aortic arch (Srivastava, 2006). *Dicer*$^{flox/flox}$ *Wnt1*^{Cre} mice also had a ventricular septal defect (Fig. 1E,J-L, arrowhead) and a discontinuance of the ascending aortic arch with the descending aorta, reflecting improper patterning of the aortic arch due to a left fourth aortic arch defect (Fig. 1O,X, asterisk). Furthermore, thymus development, which is also dependent on NCCs, was absent in *Dicer*$^{flox/flox}$ *Wnt1*^{Cre} mutants (Fig. 1M,O) and delayed in *Dicer* heterozygous embryos (*Dicer*$^{flox/+}$ *Wnt1*^{Cre}) at E14.5 (Fig. 1M,N). The haploinsufficiency of *Dicer* was transient, as the thymus was morphologically indistinguishable in wild-type and *Dicer* heterozygous embryos by E16.5. These diverse anomalies suggest that proper miRNA-mediated post-transcriptional regulation of gene expression is required for the development of NCC-derived tissues.

The severe defects in *Dicer* mutants might be caused by a failure of NCCs to delaminate from the neural tube and/or migrate properly. To address this, we crossed a Cre-dependent reporter mouse line, *R26R-YFP* (Soriano, 1999), which marks all progeny of Cre-expressing cells with yellow fluorescent protein (YFP), into the *Dicer*$^{flox/flox}$ *Wnt1*^{Cre} background. We first investigated the early migratory behavior of NCCs at E8.5 and found no gross defect in the ability of mutant NCCs to delaminate and migrate (Fig. 1P,U). Additionally, NCC migration was grossly unaffected at E9.5 (Fig. 1Q,V and see Fig. S2A,C in the supplementary material) and at E10.5 in mutants, with streams of YFP^{+} NCCs migrating towards the PAs (see Fig. S2B,D in the supplementary material, arrowheads) and normal occupancy of YFP^{+} NCCs in the PAs. YFP was expressed in the craniofacial region of E14.5 mutants, albeit at lower intensity than in wild-type littermates, suggesting that NCC progeny condensed in the proper locations (Fig. 1R,W). YFP^{+} cells also lined the aorta and common carotid arteries of mutants (Fig. 1S,X), although the transverse aorta was absent, consistent with loss of the left fourth aortic arch artery. Although we detected YFP^{+} cells in the outflow tract, these cells did not differentiate into smooth muscle in the wall of the ductus arteriosus (Fig. 1T,Y, arrows), which provides a necessary vascular connection between the aorta and pulmonary artery in the fetus. These results suggest that abnormal NCC patterning, differentiation or maintenance, rather than delamination or migration, causes the defects seen in *Dicer* mutant NCC-derived tissues.

Dlx2 expression is decreased in PA1 of *Dicer*$^{flox/flox}$ *Wnt1*^{Cre} mutant mouse embryos

Next, we investigated whether patterning or maintenance of the bilaterally symmetric PAs was defective in *Dicer*$^{flox/flox}$ *Wnt1*^{Cre} mutants. Morphologically, the emergence, size and shape of the PAs patterned along the anterior-posterior axis were indistinguishable in mutant and wild-type embryos at E10.5. However, expression of the distal-less homeobox gene (*Dlx2*), a regulator of NCC patterning in PA1 (Qiu et al., 1995), was downregulated in the mandibular and, less severely, in the maxillary portions of PA1 in mutants (Fig. 2A,D). The mandibular component of PA1 contributes to the lower jaw, whereas the maxillary region of PA1 populates the palatal region and other craniofacial bones. Other markers of NCC-derived PA mesenchyme, such as *Msx1* (Satokata and Maas, 1994), were not diminished (Fig. 2B,E). By contrast, expression of fibroblast growth factor 8 (*Fgf8*), which is required for survival of NCC-derived PA mesenchyme (Macatee et al., 2003; Trumpp et al., 1999), was also greatly downregulated in the adjacent mandibular ectoderm of PA1 in mutants (Fig. 2C,F).

To determine whether loss of *Dlx2* and *Fgf8* expression in PA1 affected NCC maintenance, we assessed cell proliferation with an anti-phospho-histone H3 antibody and apoptosis using the TUNEL assay. At E10.5, no statistically significant difference between mutant and wild-type embryos was detected by either assay (Fig. 2G,K and 2H,L; quantified in Fig. 2O,P). Concordantly, at E11.5 proliferation remained unchanged in wild-type and mutant embryos (Fig. 2I,M; quantified in Fig. 2Q); however, apoptosis increased dramatically in the PA region of the mutants (Fig. 2J,N; quantified in Fig. 2R). Thus, loss of Dicer activity in NCCs disrupted normal PA1 gene expression and the survival of NCC-derived mesenchyme.

miR-452 is enriched in neural crest cells and is sensitive to Dicer dosage

We sought to identify specific miRNAs that when disrupted could contribute to the gene expression changes in *Dicer*$^{flox/flox}$ *Wnt1*^{Cre} mutants. We searched for miRNAs enriched in normal NCC-derived PA mesenchyme. Cells from the frontonasal process and PAs of *Wnt1*^{Cre} *R26R*^{YFP} embryos were sorted into YFP^{+} (NCC) and YFP^{-} (non-NCC) populations at E10.5 and E11.5 and analyzed by miRNA microarrays. The NCC population at E10.5 was enriched for a single miRNA, miR-452, and for eight additional miRNAs at E11.5 (Fig. 3A). qRT-PCR revealed a 7-fold enrichment of miR-452 in E10.5 YFP^{+} (NCC) compared with YFP^{-} (non-NCC) populations, confirming our microarray data (Fig. 3B). Interestingly, a few miRNAs were downregulated in E10.5 NCCs heterozygous for *Dicer* (*Dicer*$^{flox/+}$ *Wnt1*^{Cre} *R26R*^{YFP}), of which miR-452 was the most downregulated (Fig. 3C). Thus, miR-452 was abundant in the NCC population and was most sensitive to the protein dosage of Dicer.

To determine the relative levels of miR-452 within PA1 compared with other regions of the embryo, we harvested E10.5 wild-type or *Dicer*$^{flox/flox}$ *Wnt1*^{Cre} mutant embryos and dissected them into PA1, midbrain region of the head, heart, limb buds, and tail to measure miR-452 levels by qRT-PCR. The qRT-PCR data revealed that miR-452 was most highly expressed in PA1 and the tail, with lower levels within the head and the limb buds, and was nearly undetectable in the heart (Fig. 3D). We observed a 60% decrease in the levels of miR-452 in PA1 of *Dicer*$^{flox/flox}$ *Wnt1*^{Cre} embryos, but not other regions of the embryo, suggesting significant expression within the NCC-derived mesenchyme of PA1 (Fig. 3D).

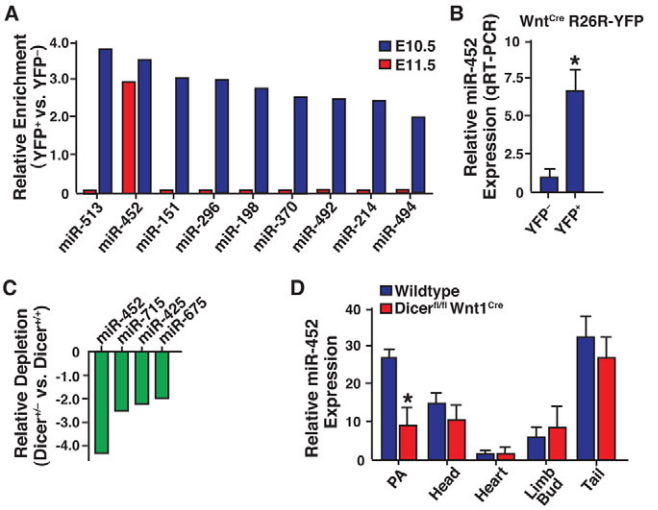

Fig. 3. miR-452 is highly enriched in NCCs and is sensitive to Dicer dosage. (**A**) NCCs (YFP^{+}) and non-NCCs (YFP^{-}) were sorted by FACS from the PA and frontonasal process regions of *Wnt1*^{Cre} *R26R*^{YFP} E10.5 and E11.5 mouse embryos. miRNA levels were measured by microarray analysis of YFP^{+} versus YFP^{-} cells. (**B**) qRT-PCR results measuring relative miR-452 expression levels from the E10.5 FACS-sorted cells in A. (**C**) NCCs (YFP^{+}) were sorted by FACS from wild-type (*Wnt1*^{Cre} *R26R*^{YFP}) and *Dicer* heterozygous (*Dicer*$^{flox/+}$ *Wnt1*^{Cre} *R26R*^{YFP}) E10.5 embryos. miRNA levels were measured by microarray analysis of heterozygous versus wild-type NCCs. (**D**) qRT-PCR results measuring relative miR-452 expression levels in the indicated tissues from E10.5 wild-type or *Dicer* mutant embryos; data were normalized to miR-452 levels in the heart. **P*<0.05. Error bars indicate 95% confidence intervals.

miR-452 regulates *Dlx2* expression in PA1

The downregulation of *Dlx2* in PA1 of *Dicer*$^{flox/flox}$ *Wnt1*^{Cre} mutant embryos provided an important assay to determine the contribution of specific miRNAs to *Dlx2* expression in the PA. We developed a Lipofectamine-based transfection approach to efficiently introduce individual mature miRNA locked nucleic acid (LNA) mimics into cultured PAs of E9.5 *Dicer*$^{flox/flox}$ *Wnt1*^{Cre} mutant embryos to test for rescue of *Dlx2* expression (Fig. 4A-C). In situ hybridization on cultured PA1 from wild type and *Dicer*$^{flox/flox}$ *Wnt1*^{Cre} mutants revealed that *Dicer*$^{flox/flox}$ *Wnt1*^{Cre} mutant PA1 exhibited *Dlx2* downregulation in culture, similar to that observed in vivo (Fig. 4D,G). We introduced mimics for five of the nine NCC-enriched miRNAs. Only miR-452 consistently rescued *Dlx2* expression in *Dicer*$^{flox/flox}$ *Wnt1*^{Cre} mutant PAs (Fig. 4J and data not shown; representative PA1s are shown in Fig. 4D-I).

We used antagomirs (Krutzfeldt et al., 2005) targeted against miR-452 to determine whether loss of miR-452 activity affects *Dlx2* expression in vivo. Antagomirs are cholesterol-modified antisense oligonucleotides that bind to and inhibit the function of endogenous miRNAs by blocking their incorporation into the RNA-induced silencing complex. Because antagomirs do not cross the placental barrier, we injected miR-452 antagomirs directly into the embryonic sac of wild-type embryos in utero. To validate this delivery method, we injected a fluorophore-modified antagomir into the embryonic sac of E8.5 embryos and observed near ubiquitous uptake of the antagomir throughout the embryos at E10.5 (Fig. 4K,L). After confirming the delivery method, we next injected miR-452 antagomir in utero at E8.5. At E11.5, miR-452 knockdown was variable and bimodal as observed by qRT-PCR (Fig. 4M). We found

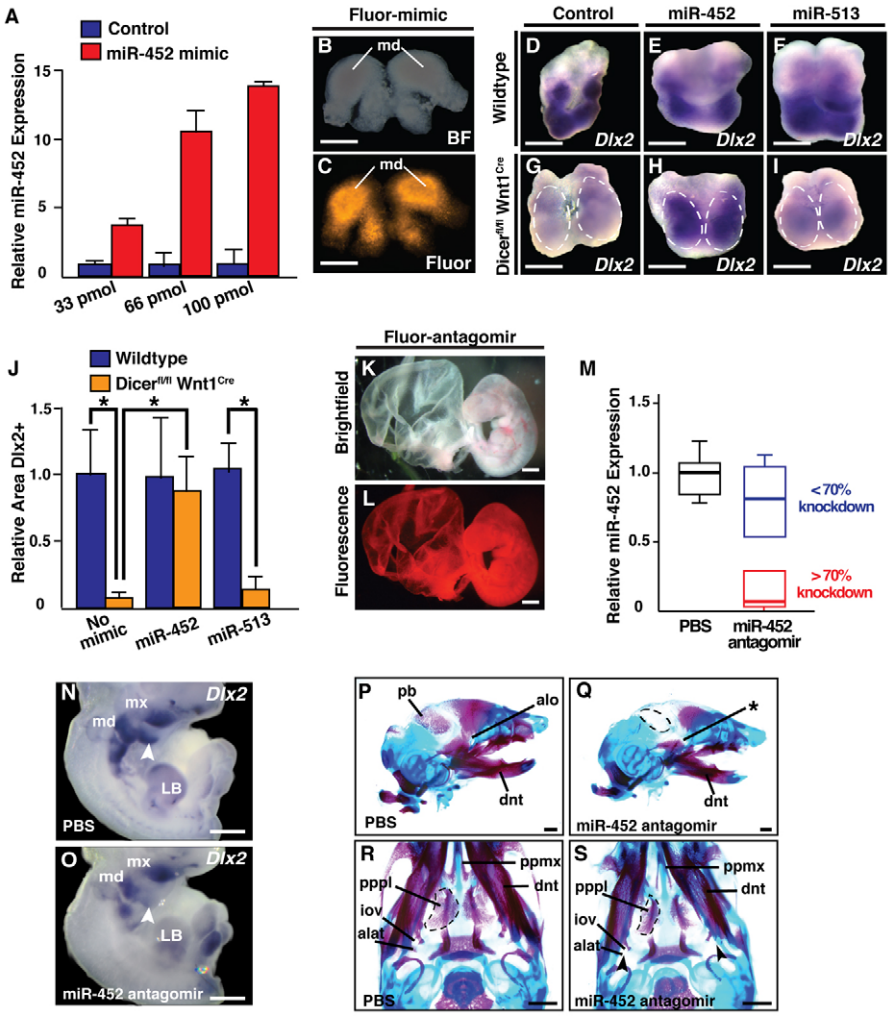

Fig. 4. miR-452 rescues *Dlx2* expression in neural crest *Dicer* mutants and is involved in craniofacial development. (**A**) qRT-PCR quantification of miR-452 levels from cultured PA1 explants transfected with increasing concentrations of locked nucleic acid miR-452 mimic or with control mimic. (**B**,**C**) Cultured PA1 explants transfected with Alexa Fluor Block-IT reagent to determine small oligo transfection efficiency via brightfield (B) and fluorescence (C) imaging to show efficiency of transfection by this technique. (**D-I**) Representative images of *Dlx2* expression in wild-type and $Dicer^{flox/flox}$ $Wnt1^{Cre}$ mutant mouse E9.5 PA1 cultures with or without overexpression of miR-452 or miR-513. (**J**) Quantification of the PA1 area that stained positive for *Dlx2* relative to the total area of the PA in *Dicer* mutants and wild-type embryos (area defined by dashed lines in G-I). The PAs were mock transfected (n=17) or transfected with a miR-452 (n=21) or miR-513 (n=9) mimic. (**K**,**L**) E8.5 embryos were transfected in utero with a fluorophore-modified antagomir and harvested at E10.5 to determine the extent of antagomir uptake in vivo. Brightfield (K) and fluorescence (L) images of injected embryos and embryonic sac showing nearly ubiquitous embryonic uptake of the fluorophore-modified antagomir. (**M**) Box plots of qRT-PCR quantification of miR-452 levels from the PA region of littermate embryos injected in utero with PBS as a control (black box, n=25) or miR-452 antagomir (blue and red boxes, n=28). Boxes represent interquartile range; the thick bar represents the median for the sample set; and error bars indicate median ± s.d. The miR-452 antagomir-injected embryos were separated into two cohorts: those with greater than 70% knockdown of miR-452 (red box; n=9) and those with less than 70% knockdown (blue box; n=19). Only those embryos with greater than 70% knockdown were considered for further study. (**N**,**O**) *Dlx2* in situ hybridization of littermate E11.5 embryos injected in utero at E8.5 with PBS (N) or miR-452 antagomir (O). Arrowhead indicates decreased *Dlx2* expression specifically in the mandibular component of PA1. (**P-S**) Alcian Blue (cartilage) and Alizarin Red (bone) skeletal staining of littermate E16.5 embryos injected in utero at E8.5 with PBS (P,R) or miR-452 antagomir (Q,S), imaged both in oblique lateral (P,Q) and ventral (R,S) views. Asterisk (Q) marks the missing cartilaginous structure, the ala orbitalis (alo). Dashed lines (Q) indicate the absence of the parietal bone (pb). md, mandibular component of PA1; mx, maxillary component of PA1; dnt, dentary; ppmx, palatal process of maxilla; iov, incisura ovale; pppl, palatal process of palatine; alat, anterolateral process of ala temporalis. Error bars in A and J indicate 95% confidence intervals. *P<0.05. Scale bars: 200 μm in B-I; 500 μm in K,L,N,O; 1 mm in P-S.

that this method of in vivo knockdown resulted in ~35% of embryos with efficient (>70%; n=9; mean=86%; median=94%) miR-452 knockdown and these embryos were used for subsequent experiments; the remainder were considered failed knockdowns.

In embryos with efficient miR-452 knockdown, *Dlx2* expression in the distal mandibular portion of PA1 in E11.5 embryos was significantly reduced, similar to that in $Dicer^{flox/flox}$ $Wnt1^{Cre}$ mutants (Fig. 4N,O). Maxillary expression of *Dlx2* was only slightly affected, consistent with what was observed in $Dicer^{flox/flox}$ $Wnt1^{Cre}$ mutants. At E16.5, some craniofacial structures of miR-452 antagomir-injected embryos were hypoplastic (Fig. 4P-S), particularly the ala orbitalis, palatal process of palatine and anterolateral process of ala temporalis (Fig. 4Q,S). Interestingly, some mesoderm-derived tissues, such as the parietal bone, were also

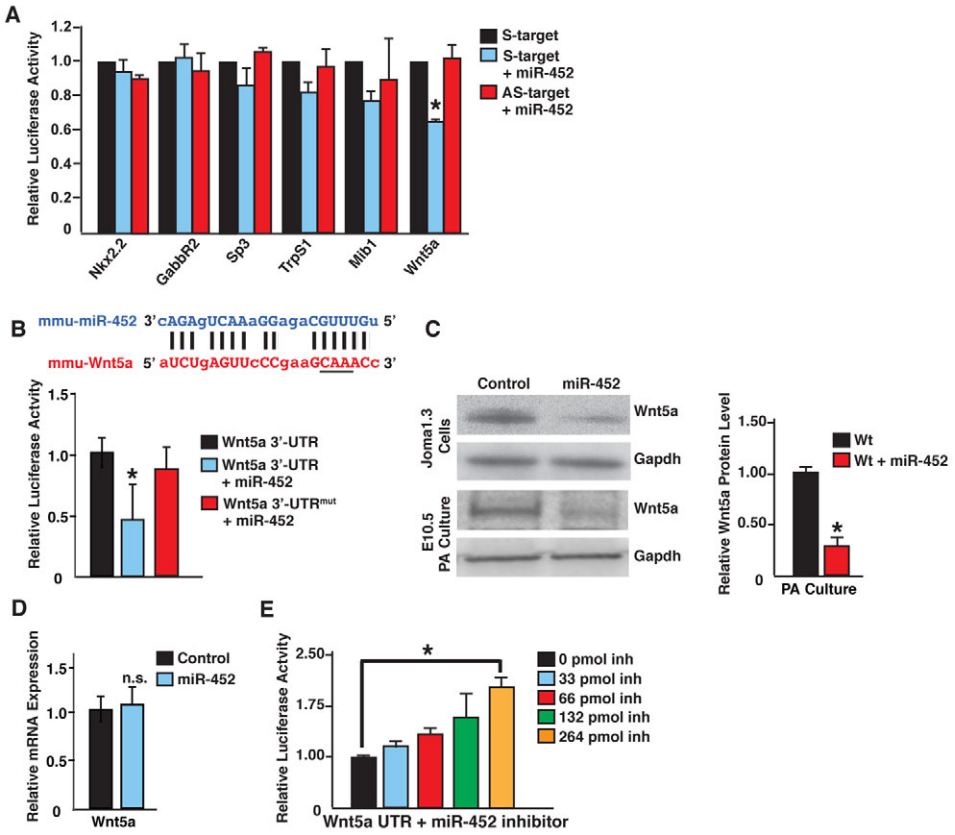

Fig. 5. miR-452 directly targets Wnt5a for repression. (**A**) Fold change in luciferase reporter activity relative to luciferase levels in the presence of the putative target 3′-UTRs in the sense orientation (S-target) or, as a control, in the antisense direction (AS-target), in JoMa1.3 neural crest stem cells (NCSCs) with or without co-transfection with miR-452 mimic. *P<0.05 versus S-target. (**B**) Putative miR-452 binding site in the mouse *Wnt5a* 3′-UTR. Vertical lines indicate sequence matches and residues mutated are underlined. Beneath is shown relative luciferase activity in the presence of the wild-type or mutant miR-452 binding site with or without miR-452 mimic in Joma1.3 NCSCs. *P<0.05. (**C**) Wnt5a protein from JoMa1.3 NCSCs or cultured wild-type E10.5 PAs transfected with or without miR-452 mimic, as assessed by western blot. Quantification of Wnt5a protein levels from western blot analysis of PAs using LI-COR software is shown to the right (n=5; *P<0.05). (**D**) Quantification of *Wnt5a* mRNA levels by qRT-PCR from NCSCs transfected with control mimic (black bar) or miR-452 mimic (blue bar). (**E**) Luciferase values from NCSCs co-transfected with a luciferase reporter vector containing the *Wnt5a* 3′-UTR and an increasing concentration of a miR-452 inhibitor (colored bars). Values were normalized to NCSCs transfected with no inhibitor (black bar). *P<0.05; n.s., not statistically significant. All experiments were performed at least in triplicate. Error bars indicate 95% confidence intervals.

affected in the antagomir-injected embryos. This finding implies that a non-NCC function of miR-452 or a non-cell-autonomous effect in the NCCs results in the disruption of mesodermal bone development. Not surprisingly, the defects resulting from miR-452 knockdown were less severe than those upon complete loss of miRNA biogenesis, reflecting the function of other miRNAs in craniofacial development or the incomplete loss of miR-452. Nevertheless, these results indicate that miR-452 is involved in proper *Dlx2* expression in NCC-derived mesenchyme and also for a subset of subsequent craniofacial development.

miR-452 directly targets *Wnt5a* and loss of miR-452 leads to decreases in Shh and Fgf8 signaling in the mandibular component of PA1

To understand the mechanism by which miR-452 regulates *Dlx2* expression, we sought to identify the direct target(s) of miR-452 in NCCs and their derivatives. Putative targets were identified with an in-house miRNA:mRNA algorithm that considers sequence specificity, binding site accessibility and evolutionary conservation of the binding site, and potential sites were then tested experimentally (Cordes et al., 2009). The neural crest stem cell (NCSC) line Joma1.3 (Maurer et al., 2007) was transfected with the miR-452 mimic along with constitutively active luciferase reporter genes containing the 3′-UTR of putative targets. Repression of luciferase activity was only observed in the presence of the *Wnt5a* 3′-UTR (Fig. 5A). Wnt5a, a non-canonical member of the Wnt family of signaling molecules, is expressed in NCC-derived mesenchyme of the PAs (Gavin et al., 1990), and its 3′-UTR contains a miR-452 binding site (Fig. 5B). Mutating the seed region of the miR-452 binding site within the Wnt5a 3′-UTR led to loss of the miR-452-dependent decrease in luciferase activity, suggesting that the activity of the predicted binding site depends on miR-452 binding (Fig. 5B). In addition to changes in luciferase activity, western blotting and qRT-PCR revealed reduced Wnt5a protein, but not mRNA, levels in NCSCs transfected with miR-452 mimics (Fig. 5C,D). We also observed a decrease in Wnt5a protein levels in our PA culture system upon transfection of miR-452 mimic (Fig. 5C). Furthermore, co-transfection of miR-452 inhibitors into NCSCs containing a luciferase vector with the *Wnt5a* 3′-UTR resulted in a dose-dependent increase in luciferase activity (Fig. 5E). These results suggest that endogenous Wnt5a protein levels are sensitive to miR-452 overexpression in vitro and in vivo.

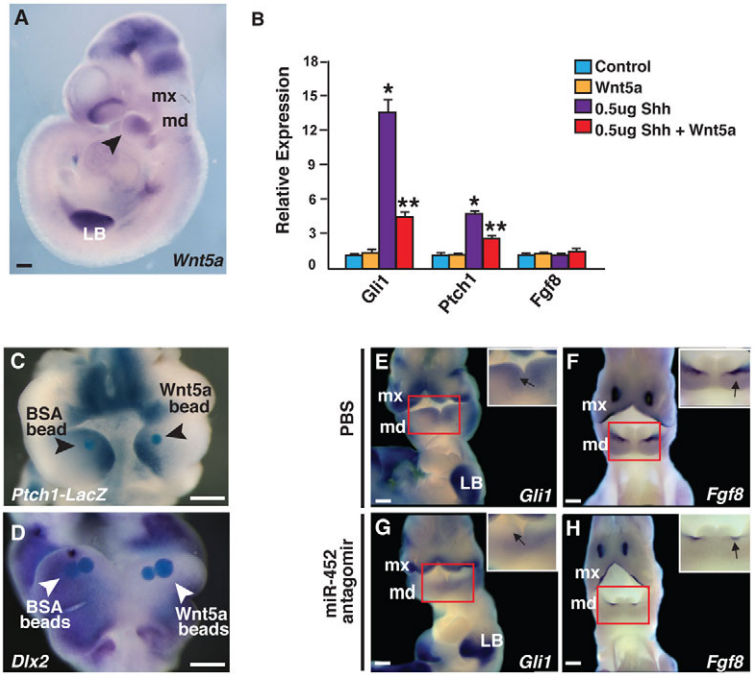

Fig. 6. Wnt5a negatively regulates Shh signaling. (**A**) Whole-mount in situ hybridization of E10.5 wild-type mouse showing expression of *Wnt5a*. Note strong expression in the mandibular component of PA1 (arrowhead). (**B**) Expression of the indicated genes as assessed by qRT-PCR in NCSCs transfected with or without an expression plasmid harboring human *WNT5A* cDNA (+Wnt5a) treated with or without 0.5 μg recombinant Shh protein. Shown is the change in gene expression relative to control (0 μg Shh). Error bars indicate 95% confidence intervals. **P*<0.05 and ***P*<0.05 versus control. (**C**) Ptch1 expression, as visualized by β-Gal staining from *Ptch1-lacZ* E10.5 mouse embryo PA explants cultured with a bead soaked in bovine serum albumin (BSA) or recombinant Wnt5a protein (arrowheads). (**D**) *Dlx2* expression, as visualized by in situ hybridization, from wild-type E10.5 mouse embryo PA explants with beads soaked in BSA or recombinant Wnt5a protein (arrowheads). Frontal view of PA is shown in C and D. (**E-H**) Whole-mount in situ hybridization for *Gli1* (E,G) and *Fgf8* (F,H) in E11.5 embryos injected at E8.5 in utero with PBS (E,F) or miR-452 antagomir (G,H) reveal downregulation of gene expression in the mandibular component of PA1 (arrows). Insets show the mandibular components of PA1 (boxed regions) at higher magnification. Scale bars: 100 μm in C,D; 250 μm in A,E-H.

In various developmental roles, Wnt5a acts as a signaling mediator of epithelial-mesenchymal interactions. For example, Wnt5a expression in lung epithelium negatively regulates *Shh* responsiveness of the underlying mesenchyme (Li et al., 2005). In PAs, Wnt5a is primarily expressed in NCC-derived mesenchyme (Gavin et al., 1990), and whole-mount in situ hybridization revealed higher levels in the mandibular component of PA1 (Fig. 6A). By contrast, Shh is produced in the pharyngeal endoderm, where it diffuses into the NCC-derived mesenchyme and activates downstream signaling cascades (Yamaguchi et al., 1999; Washington Smoak et al., 2005). Shh is required for proper development of PAs and, by positively regulating *Fgf8* expression in the pharyngeal ectoderm, supports *Dlx2* expression in the NCC-derived mesenchyme (Haworth et al., 2007; Yamagishi et al., 2006; Thomas et al., 1998).

To determine whether Wnt5a inhibits the responsiveness of NCSCs to the Shh stimulus, we transfected NCSCs with a human *WNT5A* expression plasmid, then 24 hours later treated cells with recombinant Shh protein and measured the expression levels of two Shh-responsive genes, *Gli1* and *Ptch1*. Overexpression of *Wnt5a* blunted the increase in *Gli1* and *Ptch1* mRNA expression in response to Shh treatment (Fig. 6B). To test this in vivo, we implanted beads soaked in recombinant Wnt5a or BSA (control) into PA1 of mice harboring a *lacZ* gene in the *Ptch1* locus (Goodrich et al., 1997) as a reporter of Shh signaling. β-Gal expression was decreased circumferentially around the Wnt5a bead, but not around the control bead placed in the contralateral PA (Fig. 6C). Next, we asked whether increased Wnt5a protein levels were sufficient to result in decreased *Dlx2* expression, as observed in the *Dicer* mutants and miR-452 knockdown experiments. Again, Wnt5a- and BSA-soaked beads were implanted into the mandibular component of cultured PA1 of wild-type E10.5 embryos. In-situ hybridization to assay *Dlx2* expression revealed a marked decrease in *Dlx2* expression specifically surrounding the Wnt5a-soaked beads, whereas *Dlx2* expression was unaffected surrounding the contralateral BSA-soaked beads (Fig. 6D). Thus, increased Wnt5a protein levels in the mandibular component of PA1 led to a decrease in Shh signaling and *Dlx2* expression.

We investigated whether miR-452 promotes *Dlx2* expression in part by repressing the translation of *Wnt5a*, allowing efficient Shh signaling to NCCs. Shh positively regulates expression of *Fgf8* in the pharyngeal ectoderm, and *Fgf8* expression is required for *Dlx2* expression in the NCC-derived mesenchyme (Haworth et al., 2007; Thomas et al., 2000). Thus, we hypothesized that loss of miR-452 would decrease endogenous Shh signaling and *Fgf8* expression within the endoderm and ectoderm, respectively, of PA1. Indeed, expression of *Gli1* was decreased in the mandibular component of PA1 in miR-452 antagomir-injected embryos at E11.5 and expression of *Fgf8* was markedly reduced in the mandibular ectoderm, with less of a change in the maxillary region (Fig. 6E-H). The effects of miR-452 knockdown were consistent with this miRNA participating in the reduction in mandibular *Fgf8* and *Dlx2* expression in the $Dicer^{flox/flox}$ $Wnt1^{Cre}$ mouse and the enrichment of mandibular *Wnt5a* expression. These data suggest that loss of miR-452, resulting in an increase in Wnt5a protein, leads to decreases in Shh signaling and *Fgf8* expression, which in turn result in the decrease in *Dlx2* expression seen in both *Dicer* mutant and miR-452 antagomir-injected embryos.

DISCUSSION

Here we show that miRNA biogenesis is essential for the proper development of NCC-derived tissues, including those that contribute to craniofacial, cardiovascular, thymic and nervous system structures. More importantly, we found that miR-452 was the most enriched miRNA in early NCCs and regulated epithelial-mesenchymal interactions in the mandibular region of PA1 by directly targeting Wnt5a in the NCC-derived mesenchyme. Our findings suggest that miR-452 negatively regulates secretion of Wnt5a from the NCC-derived mesenchyme of PA1, and that Wnt5a normally negatively regulates Shh signaling to the ectoderm (Fig. 7). Since Shh produced in the endoderm activates ectodermal expression of *Fgf8* (Haworth et al., 2007) and secreted Fgf8 functions to promote *Dlx2* expression in the neighboring NCC-derived mesenchyme (Thomas et al., 2000), miR-452 might regulate *Dlx2* positively in part through this complex epithelial-mesenchymal interaction. Of course, miR-452 and other NCC-

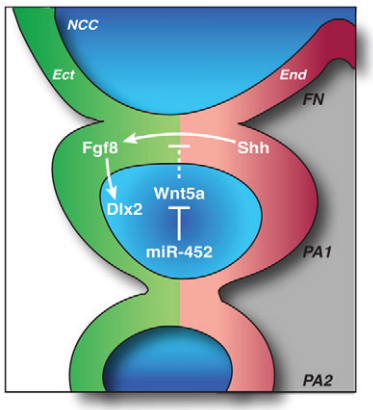

Fig. 7. miR-452 regulates *Dlx2* expression through Wnt5a, Shh and Fgf8 cross-tissue signaling. Model depicting the mechanism by which miR-452 regulates an epithelial-mesenchymal signaling cascade in PA1 that converges on *Dlx2* expression. Ect, pharyngeal ectoderm; NCC, NCC-derived mesenchyme; End, pharyngeal endoderm; FN, frontonasal cartilage. Dashed line indicates indirect regulation.

enriched miRNAs are likely to target other mRNAs in the NCC-derived mesenchyme of PA1 that further regulate the epithelial-mesenchymal interactions required for proper PA development.

In the present work, we did not address which specific NCC-enriched miRNAs function in the other arches that give rise to the thymus (PA3) or the cardiac outflow tract and aortic arch arteries (PA3, PA4 and PA6), all of which were affected in the *Dicer* mutants. One or more of the other eight NCC-enriched miRNAs is likely to contribute to the development of these structures in a stage-specific manner. Notably, the thymus and cardiac outflow tract also require cross-tissue interactions for their development and maturation (Gordon et al., 2010; Olson, 2006). For example, reciprocal signaling between the second heart field and cardiac NCCs is required for proper patterning of the aortic arch arteries (Waldo et al., 2005). Deletion of Notch signaling specifically in the second heart field leads to altered NCC behavior, resulting in a decrease of NCC-derived tissue in the outflow tract and improper patterning of the arch arteries (High et al., 2009). Other NCC-enriched miRNAs probably regulate similar pathways to coordinate the complex tissue-tissue interactions required to pattern the outflow tract and aortic arch arteries.

Interestingly, the phenotype of the $Dicer^{flox/flox}$ $Wnt1^{Cre}$ mutant mice has similarities to the human disease DiGeorge syndrome (DGS). DGS patients typically present with craniofacial, cardiovascular and thymic anomalies arising from a 3-Mb deletion of chromosome 22q11 (Lindsay, 2001). In that region, *Tbx1* has been strongly implicated in the etiology of DGS. However, *Tbx1* is not expressed in NCCs; rather, it is expressed in the pharyngeal ectoderm, endoderm and early second heart field progenitors (Merscher et al., 2001; Yamagishi et al., 2003). Tbx1 is downstream of Shh in the pharyngeal endoderm and regulates the expression of *Fgf8*, resulting in a secondary effect on the adjacent neural crest-derived mesenchyme that expresses Fgf receptors (Arnold et al., 2006; Garg et al., 2001; Hu et al., 2004; Zhang et al., 2005). Another intriguing gene in the DGS-deleted region is *DGCR8*, which is required for miRNA biogenesis (Gregory et al., 2004), and thus suggests a possible contribution of miRNA dysregulation in DGS. Our finding that $Dicer^{flox/+}$ $Wnt1^{Cre}$ heterozygous embryos have hypoplastic thymus primordia indicates that a hemizygous deletion of members of the miRNA biogenesis pathway in NCCs might result in predisposition to some DGS-like phenotypes.

Disruption of cross-tissue signaling cascades has been found in a number of human neural crest disorders (Lindsay et al., 2001; Ornitz and Marie, 2002). The results presented here suggest a crucial role for miRNAs in titrating such reciprocal signaling during NCC development and might have implications for the potential contribution of miRNA dysregulation in human neural crest disorders.

Acknowledgements

We thank B. Harfe and M. McManus for $Dicer^{flox/flox}$ mice; J. Maurer for the JoMa neural crest stem cell line; J. Reiter for *Gli1* in situ hybridization probes; Y. Huang for performing antagomir injections; J. Fish and C. Miller for histopathology support; G. Howard and S. Ordway for scientific editing; B. Taylor for manuscript preparation; and members of the D.S. lab for helpful discussion. D.S. was supported by grants from the NHLBI/NIH and the California Institute for Regenerative Medicine (C.I.R.M.). This work was also supported by NIH/NCRR grant C06 RR018928 to the Gladstone Institutes. Deposited in PMC for release after 12 months.

Competing interests statement

The authors declare no competing financial interests.

Supplementary material

Supplementary material for this article is available at
http://dev.biologists.org/lookup/suppl/doi:10.1242/dev.052647/-/DC1

References

Arnold, J. S., Werling, U., Braunstein, E. M., Liao, J., Nowotschin, S., Edelmann, W., Hebert, J. M. and Morrow, B. E. (2006). Inactivation of Tbx1 in the pharyngeal endoderm results in 22q11DS malformations. *Development* **133**, 977-987.

Bartel, D. P. (2009). MicroRNAs: target recognition and regulatory functions. *Cell* **136**, 215-233.

Cordes, K. R., Sheehy, N. T., White, M. P., Berry, E. C., Morton, S. U., Muth, A. N., Lee, T.-H., Miano, J. M., Ivey, K. N. and Srivastava, D. (2009). miR-145 and miR-143 regulate smooth muscle cell fate and plasticity. *Nature* **460**, 705-710.

Danielian, P. S., Muccino, D., Rowitch, D. H., Michael, S. K. and McMahon, A. P. (1998). Modification of gene activity in mouse embryos in utero by a tamoxifen-inducible form of Cre recombinase. *Curr. Biol.* **8**, 1323-1326.

Epstein, J. A. and Parmacek, M. S. (2005). Recent advances in cardiac development with therapeutic implications for adult cardiovascular disease. *Circulation* **112**, 592-597.

Garg, V., Yamagishi, C., Hu, T., Kathiriya, I. S., Yamagishi, H. and Srivastava, D. (2001). Tbx1, a DiGeorge syndrome candidate gene, is regulated by sonic hedgehog during pharyngeal arch development. *Dev. Biol.* **235**, 62-73.

Gavin, B. J., McMahon, J. A. and McMahon, A. P. (1990). Expression of multiple novel Wnt-1/int-1-related genes during fetal and adult mouse development. *Genes Dev.* **4**, 2319-2332.

Gentleman, R. C., Carey, V. J., Bates, D. M., Bolstad, B., Dettling, M., Dudoit, S., Ellis, B., Gautier, L., Ge, Y., Gentry, J. et al. (2004). Bioconductor: open software development for computational biology and bioinformatics. *Genome Biol.* **5**, R80.

Goodrich, L. V., Milenkovic, L., Higgins, K. M. and Scott, M. P. (1997). Altered neural cell fates and medulloblastoma in mouse patched mutants. *Science* **277**, 1109-1113.

Gordon, J., Patel, S. R., Mishina, Y. and Manley, N. R. (2010). Evidence for an early role for BMP4 signaling in thymus and parathyroid morphogenesis. *Dev. Biol.* **339**, 141-154.

Gregory, R. I., Yan, K. P., Amuthan, G., Chendrimada, T., Doratotaj, B., Cooch, N. and Shiekhattar, R. (2004). The Microprocessor complex mediates the genesis of microRNAs. *Nature* **432**, 235-240.

Harfe, B. D., McManus, M. T., Mansfield, J. H., Hornstein, E. and Tabin, C. J. (2005). The RNaseIII enzyme Dicer is required for morphogenesis but not patterning of the vertebrate limb. *Proc. Natl. Acad. Sci. USA* **102**, 10898-10903.

Harris, K. S., Zhang, Z., McManus, M. T., Harfe, B. D. and Sun, X. (2006). Dicer function is essential for lung epithelium morphogenesis. *Proc. Natl. Acad. Sci. USA* **103**, 2208-2213.

Haworth, K. E., Wilson, J. M., Grevellec, A., Cobourne, M. T., Healy, C., Helms, J. A., Sharpe, P. T. and Tucker, A. S. (2007). Sonic hedgehog in the pharyngeal endoderm controls arch pattern via regulation of Fgf8 in head ectoderm. *Dev. Biol.* **303**, 244-258.

Helms, J. A. and Schneider, R. A. (2003). Cranial skeletal biology. *Nature* **423**, 326-331.
High, F. A., Jain, R., Stoller, J. Z., Antonucci, N. B., Lu, M. M., Loomes, K. M., Kaestner, K. H., Pear, W. S. and Epstein, J. A. (2009). Murine Jagged1/Notch signaling in the second heart field orchestrates Fgf8 expression and tissue-tissue interactions during outflow tract development. *J. Clin. Invest.* **119**, 1986-1996.
Hu, T., Yamagishi, H., Maeda, J., McAnally, J., Yamagishi, C. and Srivastava, D. (2004). Tbx1 regulates fibroblast growth factors in the anterior heart field through a reinforcing autoregulatory loop involving forkhead transcription factors. *Development* **131**, 5491-5502.
Jiang, X., Rowitch, D. H., Soriano, P., McMahon, A. P. and Sucov, H. M. (2000). Fate of the mammalian cardiac neural crest. *Development* **127**, 1607-1616.
Kameda, Y. (2009). Hoxa3 and signaling molecules involved in aortic arch patterning and remodeling. *Cell Tissue Res.* **336**, 165-178.
Kobayashi, T., Lu, J., Cobb, B. S., Rodda, S. J., McMahon, A. P., Schipani, E., Merkenschlager, M. and Kronenberg, H. M. (2008). Dicer-dependent pathways regulate chondrocyte proliferation and differentiation. *Proc. Natl. Acad. Sci. USA* **105**, 1949-1954.
Krutzfeldt, J., Rajewsky, N., Braich, R., Rajeev, K. G., Tuschl, T., Manoharan, M. and Stoffel, M. (2005). Silencing of microRNAs in vivo with 'antagomirs'. *Nature* **438**, 685-689.
Le Douarin, N. M., Creuzet, S., Couly, G. and Dupin, E. (2004). Neural crest cell plasticity and its limits. *Development* **131**, 4637-4650.
Lee, H. Y., Kleber, M., Hari, L., Brault, V., Suter, U., Taketo, M. M., Kemler, R. and Sommer, L. (2004a). Instructive role of Wnt/beta-catenin in sensory fate specification in neural crest stem cells. *Science* **303**, 1020-1023.
Lee, J., Platt, K. A., Censullo, P. and Ruiz i Altaba, A. (1997). Gli1 is a target of Sonic hedgehog that induces ventral neural tube development. *Development* **124**, 2537-2552.
Lee, Y. S., Nakahara, K., Pham, J. W., Kim, K., He, Z., Sontheimer, E. J. and Carthew, R. W. (2004b). Distinct roles for Drosophila Dicer-1 and Dicer-2 in the siRNA/miRNA silencing pathways. *Cell* **117**, 69-81.
Li, C., Hu, L., Xiao, J., Chen, H., Li, J. T., Bellusci, S., Delanghe, S. and Minoo, P. (2005). Wnt5a regulates Shh and Fgf10 signaling during lung development. *Dev. Biol.* **287**, 86-97.
Lindsay, E. A. (2001). Chromosomal microdeletions: dissecting del22q11 syndrome. *Nat. Rev. Genet.* **2**, 858-868.
Lindsay, E. A., Vitelli, F., Su, H., Morishima, M., Huynh, T., Pramparo, T., Jurecic, V., Ogunrinu, G., Sutherland, H. F., Scambler, P. J. et al. (2001). Tbx1 haploinsufficieny in the DiGeorge syndrome region causes aortic arch defects in mice. *Nature* **410**, 97-101.
Macatee, T. L., Hammond, B. P., Arenkiel, B. R., Francis, L., Frank, D. U. and Moon, A. M. (2003). Ablation of specific expression domains reveals discrete functions of ectoderm- and endoderm-derived FGF8 during cardiovascular and pharyngeal development. *Development* **130**, 6361-6374.
Maurer, J., Fuchs, S., Jager, R., Kurz, B., Sommer, L. and Schorle, H. (2007). Establishment and controlled differentiation of neural crest stem cell lines using conditional transgenesis. *Differentiation* **75**, 580-591.
McLeod, M. J. (1980). Differential staining of cartilage and bone in whole mouse fetuses by alcian blue and alizarin red S. *Teratology* **22**, 299-301.
Merscher, S., Funke, B., Epstein, J. A., Heyer, J., Puech, A., Lu, M. M., Xavier, R. J., Demay, M. B., Russell, R. G., Factor, S. et al. (2001). TBX1 is responsible for cardiovascular defects in velo-cardio-facial/DiGeorge syndrome. *Cell* **104**, 619-629.
Meulemans, D. and Bronner-Fraser, M. (2004). Gene-regulatory interactions in neural crest evolution and development. *Dev. Cell* **7**, 291-299.
Meyers, E. N. and Martin, G. R. (1999). Differences in left-right axis pathways in mouse and chick: functions of FGF8 and SHH. *Science* **285**, 403-406.
Olson, E. N. (2006). Gene regulatory networks in the evolution and development of the heart. *Science* **313**, 1922-1927.
Ornitz, D. M. and Marie, P. J. (2002). FGF signaling pathways in endochondral and intramembranous bone development and human genetic disease. *Genes Dev.* **16**, 1446-1465.
Qiu, M., Bulfone, A., Martinez, S., Meneses, J. J., Shimamura, K., Pedersen, R. A. and Rubenstein, J. L. (1995). Null mutation of Dlx-2 results in abnormal morphogenesis of proximal first and second branchial arch derivatives and abnormal differentiation in the forebrain. *Genes Dev.* **9**, 2523-2538.
Riddle, R. D., Johnson, R. L., Laufer, E. and Tabin, C. (1993). Sonic hedgehog mediates the polarizing activity of the ZPA. *Cell* **75**, 1401-1416.
Satokata, I. and Maas, R. (1994). Msx1 deficient mice exhibit cleft palate and abnormalities of craniofacial and tooth development. *Nat. Genet.* **6**, 348-356.
Sauka-Spengler, T. and Bronner-Fraser, M. (2008). A gene regulatory network orchestrates neural crest formation. *Nat. Rev. Mol. Cell Biol.* **9**, 557-568.
Soriano, P. (1999). Generalized lacZ expression with the ROSA26 Cre reporter strain. *Nat. Genet.* **21**, 70-71.
Srivastava, D. (2006). Making or breaking the heart: from lineage determination to morphogenesis. *Cell* **126**, 1037-1048.
Stemple, D. L. and Anderson, D. J. (1992). Isolation of a stem cell for neurons and glia from the mammalian neural crest. *Cell* **71**, 973-985.
Thomas, B. L., Liu, J. K., Rubenstein, J. L. and Sharpe, P. T. (2000). Independent regulation of Dlx2 expression in the epithelium and mesenchyme of the first branchial arch. *Development* **127**, 217-224.
Thomas, T., Kurihara, H., Yamagishi, H., Kurihara, Y., Yazaki, Y., Olson, E. N. and Srivastava, D. (1998). A signaling cascade involving endothelin-1, dHAND and msx1 regulates development of neural-crest-derived branchial arch mesenchyme. *Development* **125**, 3005-3014.
Trainor, P. A., Ariza-McNaughton, L. and Krumlauf, R. (2002). Role of the isthmus and FGFs in resolving the paradox of neural crest plasticity and prepatterning. *Science* **295**, 1288-1291.
Trowell, O. A. (1954). A modified technique for organ culture in vitro. *Exp. Cell Res.* **6**, 246-248.
Trumpp, A., Depew, M. J., Rubenstein, J. L., Bishop, J. M. and Martin, G. R. (1999). Cre-mediated gene inactivation demonstrates that FGF8 is required for cell survival and patterning of the first branchial arch. *Genes Dev.* **13**, 3136-3148.
van Rooij, E., Sutherland, L. B., Qi, X., Richardson, J. A., Hill, J. and Olson, E. N. (2007). Control of stress-dependent cardiac growth and gene expression by a microRNA. *Science* **316**, 575-579.
Waldo, K. L., Hutson, M. R., Stadt, H. A., Zdanowicz, M., Zdanowicz, J. and Kirby, M. L. (2005). Cardiac neural crest is necessary for normal addition of the myocardium to the arterial pole from the secondary heart field. *Dev. Biol.* **281**, 66-77.
Washington Smoak, I., Byrd, N. A., Abu-Issa, R., Goddeeris, M. M., Anderson, R., Morris, J., Yamamura, K., Klingensmith, J. and Meyers, E. N. (2005). Sonic hedgehog is required for cardiac outflow tract and neural crest cell development. *Dev. Biol.* **283**, 357-372.
Yamagishi, C., Yamagishi, H., Maeda, J., Tsuchihashi, T., Ivey, K., Hu, T. and Srivastava, D. (2006). Sonic hedgehog is essential for first pharyngeal arch development. *Pediatr. Res.* **59**, 349-354.
Yamagishi, H., Maeda, J., Hu, T., McAnally, J., Conway, S. J., Kume, T., Meyers, E. N., Yamagishi, C. and Srivastava, D. (2003). Tbx1 is regulated by tissue-specific forkhead proteins through a common Sonic hedgehog-responsive enhancer. *Genes Dev.* **17**, 269-281.
Yamaguchi, T. P., Bradley, A., McMahon, A. P. and Jones, S. (1999). A Wnt5a pathway underlies outgrowth of multiple structures in the vertebrate embryo. *Development* **126**, 1211-1223.
Yang, Y. H., Dudoit, S., Luu, P., Lin, D. M., Peng, V., Ngai, J. and Speed, T. P. (2002). Normalization for cDNA microarray data: a robust composite method addressing single and multiple slide systematic variation. *Nucleic Acids Res.* **30**, e15.
Yi, R., Pasolli, H. A., Landthaler, M., Hafner, M., Ojo, T., Sheridan, R., Sander, C., O'Carroll, D., Stoffel, M., Tuschl, T. et al. (2009). DGCR8-dependent microRNA biogenesis is essential for skin development. *Proc. Natl. Acad. Sci. USA* **106**, 498-502.
Zehir, A., Hua, L. L., Maska, E. L., Morikawa, Y. and Cserjesi, P. (2010). Dicer is required for survival of differentiating neural crest cells. *Dev. Biol.* **340**, 459-467.
Zhang, Z., Cerrato, F., Xu, H., Vitelli, F., Morishima, M., Vincentz, J., Furuta, Y., Ma, L., Martin, J. F., Baldini, A. et al. (2005). Tbx1 expression in pharyngeal epithelia is necessary for pharyngeal arch artery development. *Development* **132**, 5307-5315.
Zhao, Y., Ransom, J. F., Li, A., Vedantham, V., von Drehle, M., Muth, A. N., Tsuchihashi, T., McManus, M. T., Schwartz, R. J. and Srivastava, D. (2007). Dysregulation of cardiogenesis, cardiac conduction, and cell cycle in mice lacking miRNA-1-2. *Cell* **129**, 303-317.